Nanostructured Ferroelectrics: Fabrication and Structure–Property Relations

Hee Han, Yunseok Kim, Marin Alexe, Dietrich Hesse, and Woo Lee**

With the continued demand for ultrahigh density ferroelectric data storage applications, it is becoming increasingly important to scale the dimension of ferroelectrics down to the nanometer-scale region and to thoroughly understand the effects of miniaturization on the materials properties. Upon reduction of the physical dimension of the material, the change in physical properties associated with size reduction becomes extremely difficult to characterize and to understand because of a complicated interplay between structures, surface properties, strain effects from substrates, domain nucleation, and wall motions. In this Review, the recent progress in fabrication and structure-property relations of nanostructured ferroelectric oxides is summarized. Various fabrication approaches are reviewed, with special emphasis on a newly developed stencil-based method for fabricating ferroelectric nanocapacitors, and advantages and limitations of the processes are discussed. Stress-induced evolutions of domain structures upon reduction of the dimension of the material and their implications on the electrical properties are discussed in detail. Distinct domain nucleation, growth, and propagation behaviors in nanometer-scale ferroelectric capacitors are discussed and compared to those of micrometer-scale counterparts. The structural effect of ferroelectric nanocapacitors on the domain switching behavior and cross-talk between neighboring capacitors under external electric field is reviewed.

1. Introduction

Ferroelectricity is a property of materials that means they exhibit spontaneous electric polarization that can be reversed by an external electric field. Ferroelectric materials are required by symmetry considerations to be also piezoelectric and pyroelectric. Since the discovery of ferroelectricity in Rochelle salt by Valasek in 1920[1] and in $BaTiO_3$,[2] ferroelectric complex oxides have been extensively investigated due to their attractive physical properties that can be exploited for many real-life applications.[3–9] Most applications of ferroelectric oxides are based on the simple capacitor structure, in which a ferroelectric material is sandwiched between a pair of electrodes. The high dielectric permittivity of ferroelectrics has been utilized to make capacitors with tunable capacitance, the physical sizes of which are much smaller than those of conventional dielectric (non-tunable) capacitors of comparable capacitance. Pyroelectricity originating from a temperature dependence of the spontaneous polarization has been utilized for ultrasensitive infrared detectors. On the other hand, piezoelectricity has made materials applicable to high-performance actuators, vibration sensors, and other devices. Among the many attractive physical properties of ferroelectric oxides, the reversible spontaneous electric polarization has recently attracted much attention, especially in the research field aimed at non-volatile data storage devices.

With ever-increasing demand on portable consumer electronic devices with ultrahigh-density data storage and low power consumption, the miniaturization of ferroelectric capacitors has become an important issue. It has been equally important to understand the effects of size reduction on the ferroelectric properties. Upon reduction of the physical dimension of the material, however, understanding the fundamental physics becomes extremely difficult because of a complicated interplay between surface properties, strain effects from substrates, and size reduction. To thoroughly understand the basic physics of nanostructured ferroelectrics, size effects originating not only from the thickness of the material, but also from the lateral dimension need to be investigated, i.e., both thickness and the lateral size effects.

Most previous studies on the thickness-related size effect have been dedicated to 2D ultrathin films. This research trend originated from the recent large advances in electrical characterization, relevant theories, and deposition techniques. The latter involve, e.g., in situ controlled molecular beam epitaxy (MBE) and pulsed laser deposition (PLD) combined with reflection high energy electron diffraction (RHEED).[10–17] It has been experimentally and theoretically explored that periodic domains

Dr. H. Han, Prof. W. Lee
Korea Research Institute of Standards and Science (KRISS)
Yuseong, 305-340 Daejeon, Korea
E-mail: h2m2h00@kriss.re.kr; woolee@kriss.re.kr
Dr. Y. Kim,[+] Dr. M. Alexe, Prof. D. Hesse
Max Planck Institute of Microstructure Physics
Weinberg 2, 06120 Halle, Germany
Prof. W. Lee
Department of Nano Science
University of Science and Technology (UST)
Yuseong, 305-333 Daejeon, Korea
[+] Present address: The Center for Nanophase Materials Sciences, Oak Ridge National Laboratory, Oak Ridge, TN 37831, USA

DOI: 10.1002/adma.201102249

with opposite polarization direction and conducting electrodes can stabilize ferroelectricity, even in ferroelectric films with a thickness of three and six perovskite unit cells, which indicates that a fundamental limit on the thickness of ferroelectric thin films has been overcome or may not exist.[12,17] However, only a few studies focusing on the lateral size effect have been reported because of the difficulties not only in fabricating structurally well-defined ferroelectric nanostructures, but also in characterizing the physical properties on the nanometer length scale.[18–22]

This article gives an overview on recent advances in nanostructured ferroelectric complex oxides, focusing on the fabrication and the structure–property relationships of nanocapacitors and nanoislands. Various approaches that have been employed so far for the fabrication of ferroelectric nanostructures are reviewed and the advantages and limitations of the respective processes are discussed. A promising approach for the realization of extended arrays of ferroelectric nanocapacitors is presented. The strain-induced evolution of domain structures in 2D continuous ferroelectric thin films and 0D discrete ferroelectric nanodots and its implications for the electrical properties, such as piezoresponse, are discussed. Individual data addressability, retention, and switching uniformity of extended arrays of ferroelectric nanocapacitors are presented. Domain switching in nanometer-scale ferroelectric capacitors was observed to be different from that of micrometer-scale counterparts. A recently proposed phenomenological model that may explain domain nucleation, growth, and propagation in ferroelectric nanocapacitors is presented. The discussion also covers cross-talk between neighboring nanocapacitors under external bias, which should be systematically investigated for a successful development of reliable non-volatile data storage devices.

Hee Han is a postdoc in the group of the Nanomaterials Research Laboratory at the Korea Research Institute of Standards and Science (KRISS). He received his Ph.D. degree from Pohang University of Science and Technology (Department of Materials Science) in 2010. His research focused on the fabrication of ferroelectric nanostructures and investigation of their size effects. At KRISS, he is working on development of resistive memory capacitors.

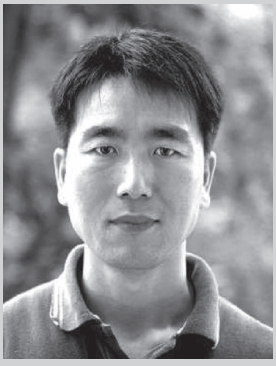

Woo Lee is a principal researcher at the Korea Research Institute of Standards and Science (KRISS) and Associate Professor of the Department of Nano Science, University of Science and Technology (UST), Daejeon, Korea. He received his Ph.D. from Seoul National University (2003). From 2003 to 2007, he worked with Prof. Kornelius Nielsch as a postdoc and then with the late Prof. Ulrich Gösele as a staff researcher at the MPI-Halle. His research interests include anodization electrochemistry of valve metals and growth mechanisms and structure–property relationships of low-dimensional materials, as well as their applications to memory and energy-harvesting devices.

2. Fabrication of Ferroelectric Nanostructures

The electrical properties of nanostructured ferroelectric oxides are very sensitive to the compositional homogeneity, the crystalline quality, and the physical dimension of materials.[18–25] For thorough understanding of the intrinsic properties of nanostructured ferroelectrics, one should be able to control the shape and size of the materials at will, engineer the lattice strain at the interface of a ferroelectric oxide and the underlying substrate, and arrange materials on a substrate of considerably large size for practical applications of ferroelectrics to ultrahigh density non-volatile memories. Correspondingly, the fabrication approach should meet the following basic requirements: i) the method itself needs to be cheap and easily accessible, allowing for an easy control of the size and shape in the sub-one-hundred nanometer region as well as mass production of desired structures with a narrow size distribution and ii) the approach is required to be high-temperature compatible. To date, various approaches have been employed for the fabrication of structurally well-defined ferroelectric nanostructures.[26–60] The fabrication strategies so far can be classified into two broad groups: top-down and bottom-up approaches. In the following sections, we give an overview on some of the recent advances in the fabrication of nanostructured ferroelectric oxides. We discuss the advantages and limitations of the conventional top-down and bottom-up approaches. Some attempts to resolve the issues in conventional nanofabrication processes will also be discussed, focusing on our recent approach to realize extended 2D arrays of ferroelectric nanocapacitors by properly combining the various merits of conventional processes. Various approaches for fabrication of nanostructured ferroelectrics of nanocapacitor and nanoisland types are summarized in **Table 1**.

2.1. Top-Down Approaches

Top-down approaches are based on the reduction of feature size through etching or removal of material from a large structure. The approach mainly relies on lithography processes by utilizing energetic particles such as photons, ions, or electron beams. It includes focused ion beam (FIB) milling and electron beam (EB) direct writing (EBDW) of a metalorganic precursor film followed by high-temperature annealing for crystallization as shown in **Figure 1**.[26–33]

The FIB technique is one of the most popular methods for fabricating ferroelectric nanocapacitors with controlled feature

Table 1. Various approaches for fabrication of nanostructured ferroelectrics of nanocapacitor and nanoisland types.

Approach		Advantages	Disadvantages	Minimum Size (nm)	Type	Reference
Top-down	FIB	High resolution Use of high quality film Uniform size and array	Surface damage Low throughput	70	Island Capacitor	[24,26–29]
	EBDW	High resolution Uniform size and array No etching process	Volume shrinkage Shape change Low throughput	70	Island	[24,30–32]
	EB-litho	High resolution Uniform size and array	Surface damage Low throughput Etching process	100	Island Capacitor	[33,34]
Bottom-up	CSD	Easy process Easy to generate various size and to access to extremely small size	Difficulty in uniform size, array, and shape	<10	Island	[23,24,36–42,46,48,60]
	MOCVD	Easy process Easy to generate various size and to access to extremely small size	Difficulty in uniform size, array, and shape	<10	Island	[24,37,43,44,59]
	PLD	Easy process Access to extremely small feature	Difficulty in uniform size, array and shape	<10	Island	[24,37]
Modified Bottom-up	Registered depo	Uniform size and array	Lithoprocess Low throughput	50	Island	[49,56]
	Mask-assisted depo	Uniform size and array on large area Easy process High crystallinity	Mask fabrication process	40	Island Capacitor	[50–55,64,84]
	Block copolymer	Uniform size on large area Easy process Access to extremely small feature	Difficulty in uniform array and shape	20	Island	[57,58]

size and shape (Figure 1a). The process starts with a pre-grown ferroelectric capacitor with a film stacking configuration of top electrode/ferroelectric/bottom electrode layers, which can be grown with an excellent quality by employing well-established methods, e.g., PLD or metal-organic chemical vapor deposition (MOCVD). A thin protecting layer of platinum is deposited on the entire surface of the top electrode. Subsequently, capacitors of a desired shape and feature size are generated by ion-beam milling of the chosen area down to the bottom electrode. The diameter of the ion beam can be as small as 6 nm and thus the process allows easy access to the ferroelectric nanocapacitors with feature sizes smaller than 100 nm. The advantage of FIB-based nanofabrication for practical applications of ferroelectric ultrahigh density non-volatile memories is that the process does not substantially alter the chemical composition of the starting ferroelectric material. A first successful implementation of such a FIB process was made in 1999 by Ganpule et al., who realized the fabrication of ferroelectric $Pb(Nb_{0.04}Zr_{0.28}Ti_{0.68})O_3$ and $SrBi_2Ta_2O_9$ (SBT) capacitors with sizes ranging from 1 μm^2 to 0.01 μm^2.[26] Since then, FIB has become a useful technique for investigating structure–property relations of micro- and nanoscale ferroelectrics. From comparative studies on the electrical properties, Nagarajan et al. found that FIB-processed discrete ferroelectric nanostructures exhibited an enhanced piezoresponse compared to the 2D thin film counterpart due to the reduced substrate clamping effect.[28] Schilling et al. observed quadrant-type fine 90° stripe domains in FIB-processed $BaTiO_3$ nanostructures and suggested that the observed domain evolution is a consequence of the minimization of energy associated with uncompensated surface charges.[29] In spite of such successful application examples, FIB-based nanofabrication has inherent drawbacks originating from the physical removal of complex oxide ferroelectrics and also from the serial nature of the process. High-energy massive ions employed for milling give

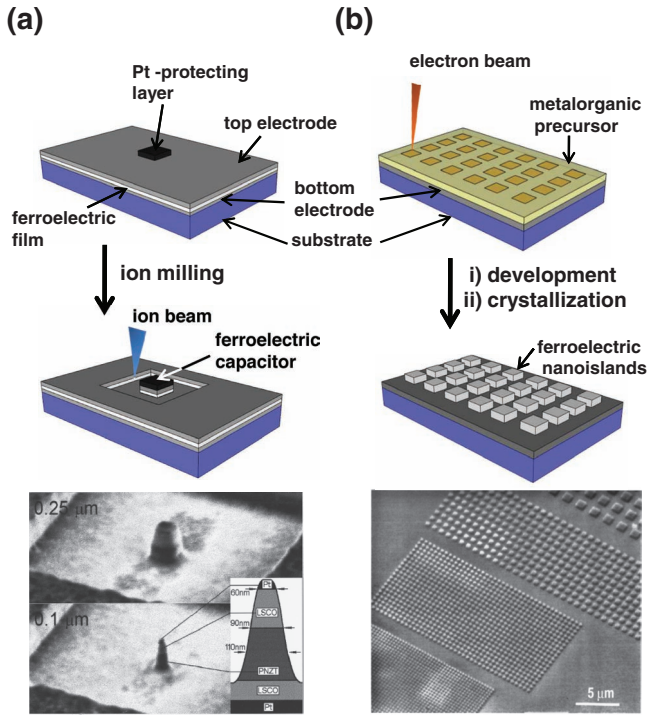

Figure 1. Two typical examples of top-down approach for nanostructured ferroelectrics: a) focused ion-beam (FIB) milling and b) EB direct writing (EBDW). Schematics of the respective nanofabrication processes (upper panel) and representative scanning electron microscopy (SEM) images of the resulting nanostructures (lower panel). Reproduced with permission.[26,30] Copyright 1999, American Institute of Physics.

rise to damage of the oxide lattice at the etched surfaces, which is the major cause of serious deterioration of electrical properties. The side surfaces of FIB-generated ferroelectric nanostructures are often contaminated with undesired materials due to redeposition of the etch products and due to an implantation of the beam material, e.g., gallium, which becomes serious as the feature size of the ferroelectrics decreases.

The EBDW technique is another useful mask-less top-down method and has widely been employed for generating metallic or oxide nanostructures (Figure 1b). The process starts with a metal-organic precursor thin film. Chemical reactions are locally induced in the metal-organic thin film by irradiation with an EB that has sufficient energy and dose, and the desired patterns are impressed by scanning the EB over the sample surface. The patterns are developed by dissolving the unexposed area in a specific solvent. Subsequently, the resulting metal-organic mesas are transformed into ferroelectric oxide by high-temperature annealing, during which a change in the original shape of the mesas takes place due to densification or volume shrinkage.[30] Alexe et al. demonstrated the fabrication of periodic patterns of ferroelectric SBT and $Pb(Zr_{0.7}Ti_{0.3})O_3$ (PZT) with a pattern density of ca. 1 Gbit cm^{-2}.[30] The generated ferroelectric nanostructures were polycrystalline with grains of 20 nm diameter or less. From piezoresponse force microscopy (PFM) investigations, they found that the fabricated ferroelectric nanoislands exhibit negative vertical shifts of the piezoelectric hysteresis loops, which was attributed to the pinned domains both at the free surface and at the ferroelectric/electrode interface.[31] The thicknesses of the pinned layers were estimated to be ca. 35 nm for the free surface and 10 nm for the ferroelectric/electrode interface. These results imply that for practical applications polycrystalline ferroelectric nanoislands need to be larger than 70 nm. Using conventional EB lithography, Bühlmann et al. fabricated PZT nanoislands with different feature sizes and found that ferroelectric nanoislands with feature sizes below 300 nm exhibit very high piezoresponse.[33] The observed enhancement in the electrical properties was attributed to the vanishing of *a*-domains in nanometer-scale ferroelectrics. The origin of such enhancement needs to be further explored by systematic investigations on the evolution of the domain structure as a function of dimensions of ferroelectric oxides in the nanometer length region.

As discussed above, top-down approaches provide a good opportunity for resolving the issues of precise positioning and tight control of the shape and size of nanostructured ferroelectrics, enabling to some extent investigations of structure–property relationships. However, enormous challenges remain to be overcome due to drawbacks originating from the serial nature of conventional top-down processes, in particular the time-consuming and low-throughput character of these processes.

2.2. Bottom-Up Approaches

Bottom-up approaches are based on naturally occurring self-assembly of atoms, molecules, or nanoparticles for the realization of ferroelectric nanostructures. The approach provides several distinct advantages over top-down based nanofabrications. It allows one to easily access the critical size of ferroelectric materials, below which ferroelectricity vanishes completely, i.e., the superparaelectric limit. In addition, the processed ferroelectric nanostructures are single crystalline and free from lattice defects near the surface. However, bottom-up based nanofabrications have limitations in terms of control of size and shape as well as precise positioning of nanoscale ferroelectrics because they rely on either thermodynamically driven reorganization or self-assembly processes.

Typical bottom-up approaches for ferroelectric nanostructures include chemical solution deposition (CSD) (**Figure 2**a) and MOCVD (Figure 2b). They utilize the microstructural instability of thin precursor films at high temperatures driven by the tendency to minimize their interface energy between the film and the underlying substrate when the film thickness is below a certain threshold.[36–42,45,46,60] The initial film thickness, the annealing temperature, and the crystallographic orientations of the substrate are known to determine both the size and shape of the resulting ferroelectric nanostructures.[38,44] In general, ferroelectric nanograins with relatively uniform size and shape can be obtained from ultrathin precursor films by high-temperature annealing for an extended period of time.

Roelofs et al. reported that CSD-grown $PbTiO_3$ (PTO) nanograins undergo a phase transition from ferroelectric to superparaelectric, losing their ferroelectricity, when their lateral

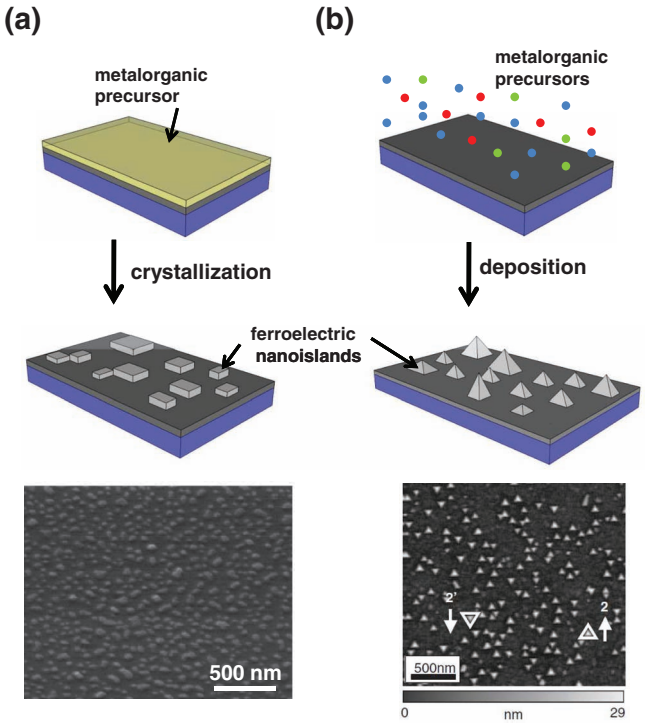

Figure 2. Two typical examples of bottom-down approach: a) chemical solution deposition (CSD) and b) metal-organic chemical vapor deposition (MOCVD). Schematics of the respective nanofabrication processes (upper panel) and representative SEM images of the resulting ferroelectric nanostructures (lower panel). SEM image in panel (a) reproduced with permission.[41] Copyright 1999, American Institute of Physics. SEM image in panel (b) reproduced with permission.[59] Copyright 2003, Japan Society of Applied Physics.

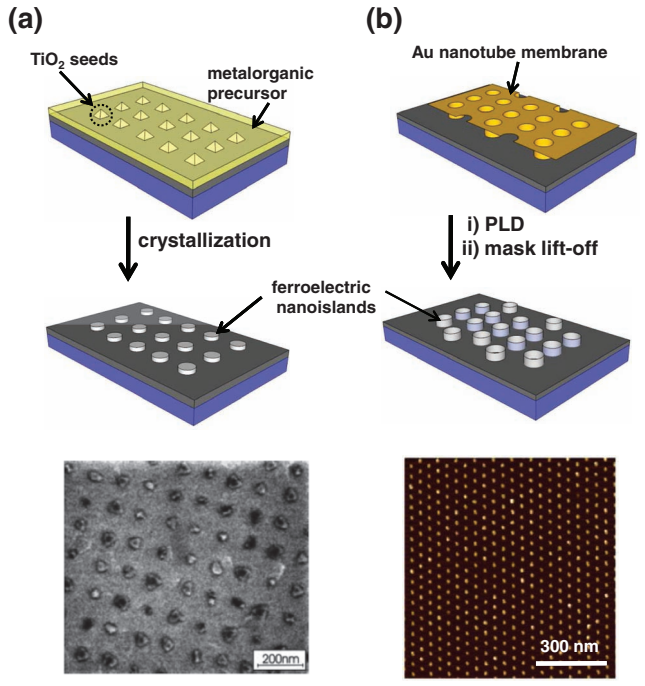

Figure 3. Selective growths of ferroelectric nanoislands via a) registered deposition and b) pulsed laser deposition (PLD) of ferroelectric materials through a gold nanotube membrane. Schematics of the respective processes (upper panel) and representative microscopy images of the resulting ferroelectric nanoislands (lower panel). AFM image in panel (a) reproduced with permission.[56] SEM image in panel (b) reproduced with permission.[52] Copyright 2005, American Institute of Physics.

sizes are below 20 nm.[40] On the other hand, Fujisawa et al. reported that even much smaller nanostructures can exhibit ferroelectricity by showing that an MOCVD-grown PTO nanoisland (thickness = 1.7 nm, diameter = 38 nm) exhibits ferroelectric polarization reversal. They further suggested that the critical volume of nanostructured PTO is in the range between 6×10^2 nm^3 and 1.9×10^3 nm^3.[43] More recently, Han et al. performed comprehensive investigations on the size effect and also on the structure–property relationships of CSD-grown PTO nanoislands by using synchrotron X-ray diffraction (XRD) and PFM. They observed a sharp increase in piezoresponse as the size of PTO decreased, which was attributed to the reduced substrate clamping effect and also to the reduced *a*-domain contribution.[45] The effect of misfit dislocations at the interface between the CSD-grown ferroelectric nanoislands and the underlying oxide substrate on the polarization instability was systematically investigated by high-resolution transmission electron microscopy (HRTEM).[46] The interfacial dislocations turned out to interact with ferroelastic twin walls, resulting in immobile twin walls under an external electric field.[60] This complex interplay of substrate clamping and interfacial dislocations should account for the low mobility of twin walls in continuous epitaxial films. Correspondingly, misfit engineering is essential for guaranteeing stable ferroelectric polarization in nanoscale ferroelectrics.

2.3. Modified Bottom-Up Approaches

There has been much effort to develop a novel method which combines advantages of both top-down and bottom-up approaches where nanosized ferroelectrics are grown selectively in predefined locations.[49–58] The selective growth can be realized by preferential registration of ferroelectric materials onto a prepatterned seed as shown in **Figure 3**a.[49,56] For the registered deposition, arrays of TiO_2 dots have been widely employed as seed patterns because TiO_2 dots trap the PbO molecules, resulting in enhanced nucleation rate for PTO. TiO_2 patterns can be easily generated by conventional EB lithography. Deposition of ferroelectric materials onto TiO_2 seed patterns was carried out by either sputtering or CSD.

Another attractive method for selective growth of ferroelectrics is a mask-assisted physical vapor deposition (PVD) as schematically shown in Figure 3b. In this approach, metal membranes with hierarchically organized arrays of nanotubes, hexagonally close-packed arrays of microspheres, and oxide membranes perforated by nanoholes can be used as stencil masks for the deposition of ferroelectric materials.[50–55] One-step deposition of ferroelectric materials through the masks simply generates 2D ordered arrays of ferroelectric nanostructures with uniform size and shape on the entire surface of the substrate, thus allowing one to utilize conventional bulk characterization tools (e.g., XRD) for structural characterization. Most recently, block-copolymer micelles have been employed

for ultrahigh density arrays of PTO nanograins with uniform diameter (≈2 nm) and thickness (≈7 nm) on a single crystal substrate. PTO precursors can be incorporated into the cores of self-ordered arrays of micelles, and transformed into crystalline ferroelectric PTO upon annealing at high temperature. PTO nanograins with extremely small volume (≈2.6×10^3 nm^3) are characterized by highly *c*-domain structures and exhibit distinct piezoresponse.[58]

The approaches mentioned above have inherent disadvantages in that they require a post-annealing process at high temperature for the crystallization of ferroelectrics. However, such a post-annealing process is often accompanied by undesired changes of shape or volume of the resulting ferroelectric nanostructures, which becomes serious as the feature size of ferroelectrics decreases.

2.4. Hard-Mask-Based Approach for Ferroelectric Nanocapacitors

Metal–insulator–metal (MIM) stacking configurations of capacitors have been mainly realized by top-down approaches, i.e., sequential depositions of metal top electrode material and oxide insulator material onto a bottom metal electrode and the milling of multilayers. Recently, Evan et al. developed a non-lithographic process to demonstrate the fabrication of ferroelectric nanocapacitors that consist of Au top-electrode/ferroelectric film/Pt hard-nanowires embedded in nanopores of anodic aluminum oxide (AAO).[61] Each Pt hard-nanowire separated by an insulating oxide matrix serves as a bottom electrode for local polarization switching in the upper ferroelectric film under an external electric field. Although the approach and demonstrated capacitor structure may be a new conceptual ferroelectric nanoscale memory, there are inherent limitations in terms of individual addressing of information on each bit and lateral-field overlapping through the ferroelectric film under external bias.[62,63]

Recently Lee et al. reported a novel process for the fabrication of physically separated ferroelectric nanocapacitors on large area with high degree of 2D spatial ordering by utilizing ultrathin AAO hard masks.[64] The excellent thermal stability of ceramic AAO masks offers an advantage in that ferroelectric materials can be in situ deposited at crystallization temperature. In addition, the facile controlling capability of pore diameter and interpore distance of the AAO provides a large degree of freedom for fabricating uniform ferroelectric nanostructures with tailor-made size and density (up to 0.2 Tbit in.$^{-2}$). In general, porous AAO masks with pore size ranging from 20 nm to 400 nm and pore density ranging from 5×10^8 cm^{-2} to 3×10^{10} cm^{-2} can conveniently be prepared by simple electrochemical oxidation of aluminum.[65] By utilizing nanoporous AAO as a mask for PLD of PZT materials, two different types of ferroelectric nanocapacitors (i.e., film-type nanocapacitors and island-type nanocapacitors) were prepared (**Figure 4**) and the structure–electrical property relationships of the respective capacitor types were systematically investigated.

A film-type nanocapacitor consists of Pt-island top electrode/PZT thin film/Pt film bottom electrode (Figure 4a). On the other hand, an island-type nanocapacitor is composed of

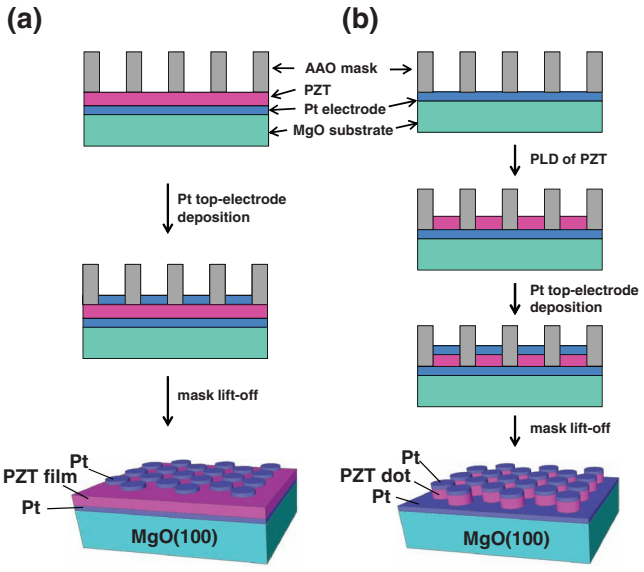

Figure 4. Schematics of fabrication procedures for two different types of PZT nanocapacitors: a) film-type nanocapacitors (Pt-top electrode island/PZT film/Pt bottom electrode) and b) island-type nanocapacitors (Pt-top electrode island/PZT dot/Pt-bottom electrode).

a Pt-island top electrode/PZT island/Pt film bottom electrode (Figure 4b). The deposition temperature was found to affect the migration of PZT particles during the PLD process. At a low temperature (e.g., 300 °C), the PZT material piles up on the surface of the nanoporous oxide mask and eventually blocks the pore mouths. At a high temperature (e.g., 500 °C), on the other hand, PLD of PZT material does not block the pore mouth due to enhanced mobility of the adsorbed PZT particles on the surface of the oxide mask. Extended arrays of PZT nanoislands on a desired substrate could be obtained by simply lifting off the stencil mask after PLD deposition.

Figure 5a,b show cross-sectional transmission electron microscopy (TEM) images of a) arrays of PZT nanoislands and b) a single PZT nanoisland that is marked with a white rectangle in panel (a). HRTEM analysis of the sample indicated that PZT nanoislands were grown epitaxially and single crystalline. Contrary to the nanostructures fabricated by conventional top-down methods, PZT nanostructures are free from lattice damage at the surface or chemical contamination because of the in situ deposition of materials at crystallization temperature followed by simple lift-off of the oxide mask.

Extended arrays of ferroelectric nanocapacitors can also be obtained by sequential deposition of materials into the nanoporous oxide mask. A representative cross-section TEM image of ferroelectric nanocapacitors with a stacking configuration of Pt/PZT/Pt on MgO(100) substrate is shown in Figure 5c, in which the interface between the 10-nm-thick Pt top-electrode and the PZT is denoted by a white solid line. The inset in Figure 5c is a fast Fourier transform image of the PZT nanoisland. Selected area electron diffraction (SAED) analysis manifested epitaxial relations between layers (i.e., PZT/Pt and Pt/MgO(100)) as shown in Figure 5d,e. The epitaxial growth and the ferroelectric phase could also be confirmed by synchrotron XRD by taking advantage of the large sample dimension.

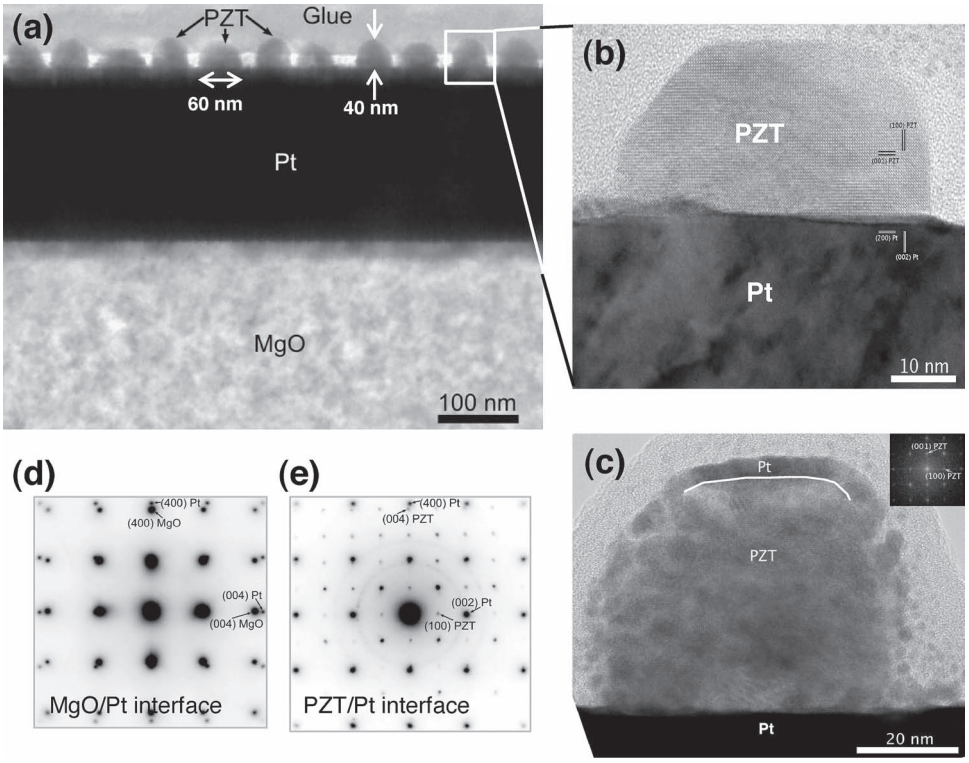

Figure 5. Cross-section TEM images of a) arrays of PZT nanoislands grown on Pt/MgO(100), b) a PZT nanoisland, and c) a Pt/PZT/Pt nanocapacitor. Selected area electron diffraction (SAED) patterns obtained from the interfaces of d) Pt/MgO and e) PZT/Pt. Reproduced with permission.[64]

3. Electrical Properties of Ferroelectric Nanocapacitors

3.1. Structure–Property Relationship in Island-Type Nanocapacitors

Ferroelectrics consist of domains where the spontaneous polarization is uniformly oriented; between the domains, domain walls exist.[66–69] In the case of tetragonal ferroelectric films grown on cubic substrates, there are two kinds of domains: *c*-domains and *a*-domains where the spontaneous polarization is out-of-plane and in-plane, respectively. Domain structures and wall movements are closely related to the electrical properties of ferroelectrics. Hence, understanding of domain structure (relative volume fraction of *c*- and *a*-domains, their spatial distributions and scaling of domain size) and domain dynamics (nucleation of domains and domain wall movement) is essential for practical applications of ferroelectrics.[70–72] In particular, as interest in nanostructured ferroelectrics increases, much attention has recently been paid to the evolution of domain structures at the nanoscale and their implications for the electrical properties. In this context, great effort has been made in the last few years to investigate the domain structures of nanostructured ferroelectrics and to characterize the electrical properties, and thus numerous papers have been published.[24,25,73–82]

The studies on nanoscale domains have been widely carried out using the PFM technique.[73,74] This technique is based on probing the strong coupling between polarization and electromechanical behavior. Because PFM is performed in AFM contact mode, where a conductive tip is electrically biased for probing electromechanical coupling, it can provide intrinsically high spatial resolution and high localization of electric field at the junction between the tip and ferroelectric surface. In addition, its easy implementation, effective manipulation, and control of nanoscale domains and local spectroscopy capabilities make it a well-suited tool for nanoscale ferroelectric studies and thus it has been giving opportunities for non-destructive visualization of domain structures in ferroelectrics and testing the electrical properties of nanoscale ferroelectric structures. One of the special characteristics of PFM is its capability to detect the polarization state through the top electrode of a ferroelectric capacitor, which makes it possible to study, on the nanoscale, the statics and dynamics of domain structure under a uniform electric field and, thus, allows the direct imaging of domain nucleation and growth and a thorough understanding of the mechanisms that govern these processes.[77]

In an attempt to study the evolution of domain structures in nanostructured ferroelectrics, recently various forms of single crystal free-standing ferroelectric nanostructures have been fabricated by direct FIB milling.[80–82] It was clearly shown by scanning TEM that the orientation of polarization is so sensitive to the local morphology of the nanostructured ferroelectrics that the local non-axial polarization direction can be controlled to a certain extent in terms of the minimization of depolarizing field. In addition, the domain size was smaller in 3D structures than in 2D thin films of comparable thickness, which suggests

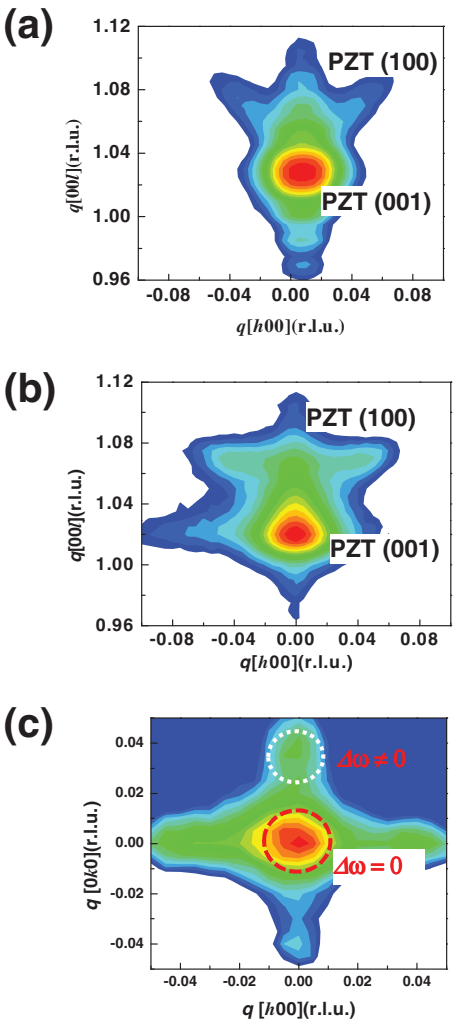

Figure 6. Contour plots obtained by reciprocal space mapping (RSM) of a) a PZT thin film grown on Pt/MgO(100), b) PZT nanoislands grown on Pt/MgO(100), obtained near the PZT (001) reflection, and c) *HK* plane mesh of PZT (100). Panel (a) reproduced with permission.[83] Copyright 2010, American Institute of Physics. Panels (b) and (c) reproduced with permission.[64]

that the role of domains and domain walls can be enhanced in the new 3D architectures, the more the scaling of domain size is correlated to the scaling in other domain-related properties such as coercive fields and switching kinetics.

The evolution of domain structures in ferroelectric 0D-islands epitaxially grown on a single crystalline underlying layer was systematically investigated by synchrotron XRD.[64,83] **Figure 6**a,b show the *HL*-plane scans of a) a 40 nm-thick PZT thin film and b) 40 nm-thick PZT nanoislands with lateral size of 60 nm grown on Pt/MgO(100). In the contour plots, PZT (001) and (100) reflections correspond to *c*-domains and *a*-domains, respectively. Both structures consist of a major fraction of *c*-domains and a minor fraction of *a*-domains. In the case of the PZT thin film, the shape of the *a*-domain reflections appears to be branching off diagonally to both sides, while the shape of the *a*-domain reflections in PZT nanoislands appears to be rather flat. This tendency has been observed in epitaxial ferroelectric films where the strain state of the film changes from compressive to tensile. Through further investigations of *a*-domain structures, it was revealed that the domain evolution in 0D discrete ferroelectric nanostructures is different from that in 2D continuous ferroelectric films as shown in Figure 6c. Unlike for the case of a continuous film where the *a*-domains are tilted by a certain angle with respect to the substrate plane to maintain the *a*/*c* twin boundary coherence,[69] discrete PZT nanoislands exhibit non-tilted *a*-domains whose [001] axes are aligned parallel to the plane of the underlying substrate.[64] This observation agrees with a recent experimental finding from 100-nm-sized $PbTiO_3$ patterns epitaxially grown on Pt/MgO(100) and can be attributed to a rather high degree of misfit strain relaxation in nanometer-sized ferroelectric islands.[84]

The role of *a*-domains is of importance because the movement of *a*-domains in ferroelectric films under external electric field is known to be able to contribute extrinsically to the ferroelectric properties. However, the switchability of *a*-domains remains still controversial. It was reported that various defects (e.g., grain boundaries or dislocations located at the film/substrate interface) or strong clamping imposed by underlying substrates can limit the switching of *a*-domains in ferroelectric thin films.[46,60,85,86] On the other hand, there are reports that evidence the switching behavior of *a*-domains in ferroelectric films under external electric field by removing the factors limiting the domain switching.[87–96] Chu et al. showed that since the interfacial dislocation core could act as a potential barrier on field-induced domain switching, stable polarization reversal could be achieved by removing the interfacial dislocations.[46] Xu et al. reported that *a*-domains could be strongly pinned in a ferroelectric film with thickness and grain size below 2 μm and 100 nm, respectively. However, as the film thickness became thicker (>5 μm) with grain size above 2 μm, then *a*-domains were found to be switched by an external electric field, leading to an extrinsic contribution to the piezoelectric properties.[85] Recently Kim et al. demonstrated that as the thickness of MOCVD-grown PZT films increased, the population of *a*-domains in the films also increased and the *a*-domains were able to be switched to *c*-domains, enabling a large contribution to the enhancement of the piezoelectric coefficient.[88] They also found that domain structures of MOCVD-grown PZT films could be divided into three different regions (i.e., a *c*-domain-dominant region with periodic arrays of twin domains, an *a*-domain-dominant region, and a mixed region with both an *a*–*c* domain structure in the upper layer and an *a* -domain structure in the lower layer). Among the three different domain regions, mixed domain structures were found to have the largest piezoelectric coefficient due to *a*-to *c*-domain switching under external electric field.[89] The elimination of substrate clamping by reducing the lateral dimension, creating discrete features, also gives rise to the displacement of *a*-domains and thus to an enhancement of the piezoelectric coefficient. As previously mentioned, Bühlman et al. showed that the enhancement of piezoresponse in submicrometer-sized PZT islands could occur due to the removal of *a*-domains during the thermal annealing.[33] Similar to this result, Nagarajan et al. showed that considerable enhancement of electrical properties in patterned PZT capacitors could occur due to the reduced substrate clamping effect in a way that *a*-domains became highly mobile and thus contributed to the

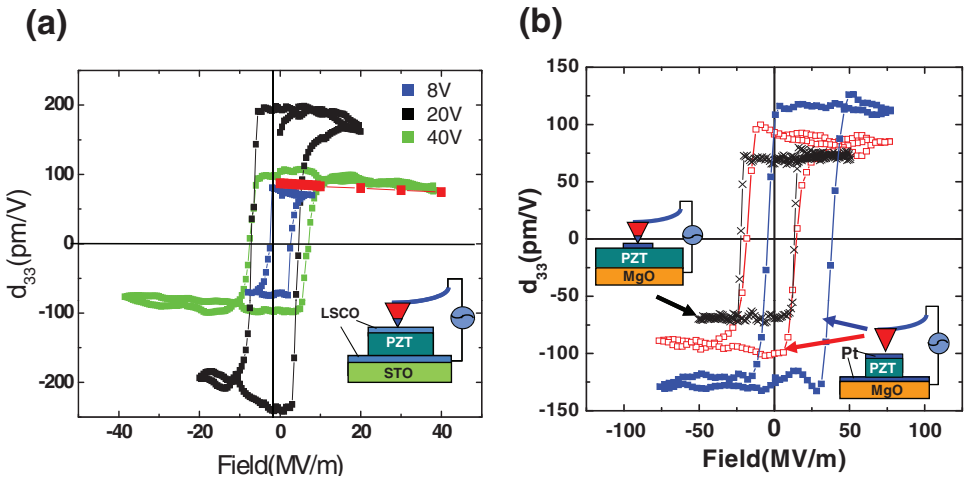

Figure 7. Piezoresponse hysteresis loops obtained by PFM measurements for a) 1 μm × 1 μm PZT island under different applied electric field and b) 65-nm-sized PZT nanocapacitor (blue and red squares for first and second hysteresis operations) and 20 μm × 20 μm PZT capacitor (cross marks). Panel (a) reproduced with permission.[28] Copyright 2003, Nature Publishing Group. Panel (b) reproduced with permission.[83] Copyright 2010, American Institute of Physics.

increase of piezoresponse.[28] **Figure 7**a shows hysteresis loops of the piezoresponse measured for a 1-μm-sized PZT nanocapacitor. The theoretically calculated piezoelectric coefficient for a single-domain bulk PZT crystal is also shown in the figure (red squares). A remnant piezoelectric coefficient of 87 pm V^{-1} was obtained by applying 8 V to the capacitor (blue squares). As the applied voltage was increased to 20 V the piezoelectric coefficient was 250 pm V^{-1} (black squares), which is three times larger than the theoretically obtained value and five times larger than the clamped value. Finally, the piezoelectric coefficient decreased to 90 pm V^{-1} under an applied voltage of 40 V due to the removal of all *a*-domains from the capacitor (green squares). By means of a simple analytical model it was also shown that the effective clamping stress level of a 100-nm-sized pattern is 100 times lower than that of a 100-μm-sized pattern.[91] Similar to the micrometer-sized ferroelectrics, the increase of piezoresponse was also observed experimentally in nanometer-sized ferroelectrics due to the strain relaxation. Lee et al. reported that 65 nm-sized PZT nanoislands (i.e., without a top electrode) had a remnant piezoelectric constant of 100 pm V^{-1}, which is comparable to theoretical values inspite of the small volume of the nanoisland due to the rather low level of strain.[64] Figure 7b shows piezoelectric hysteresis curves obtained from PZT nanocapacitors with lateral dimensions of 20 μm and 65 nm. In the case of the nanocapacitor, uniform piezoelectric excitation in the ferroelectric material can occur since the top electrode can provide a homogeneous electric field underneath the ferroelectric and the electrical contact between the PFM tip and the top electrode is improved. As shown in Figure 7b, the squareness of the piezoelectric hysteresis loop of the PZT nanocapacitor was improved compared to a PZT nanoisland without top electrode. At the first hysteresis run, the piezoelectric constant is about 130 pm V^{-1} (solid squares), which is a higher value than that of the PZT nanoisland without top electrode. During the second hysteresis run, the piezoelectric constant decreases down to 100 pm V^{-1} (open squares). This decrease of piezoelectric coefficient during the successive hysteresis operation can be attributed to the *a*-domain switching caused by the strain relaxation in the PZT nanocapacitor, similar to the experimental observation reported by Nagarajan et al. Switchable *a*-domains under external electric field are assumed to be tilted *a*-domains because the movement of non-tilted *a*-domains may be hindered by stress. The piezoelectric constant of the 65-nm-sized nanocapacitor is still 30% larger than that of the 20-μm-sized PZT capacitor (cross marks) due to the reduced substrate clamping.

3.2. Data Addressability, Uniformity, and Retention Properties of Island-Type Ferroelectric Nanocapacitors

For probe-based ferroelectric data storage media, the memory density is determined by the size of the ferroelectric units and their interdistance. Each element should be individually addressable by a conductive probe for writing and reading the data. In the probe-based data storage media the thickness of the ferroelectric film and its coercive voltage should be small enough for avoiding an overlapping of the electric field between individual neighboring bits through the continuous ferroelectric medium.[61] Woo et al. reported that the minimum stable bit size would be equal to the film thickness, which means that the density of data storage could be determined by the thickness of the ferroelectric.[92] However, ultrathin ferroelectric films turned out to lead to significant size effects, such as suppression of Curie temperature or domain pinning due to the depolarizing field.[10,16] It was also reported that in the case of film-type capacitor configurations, reducing the lateral dimension causes the coercive field to increase so significantly that it becomes impossible to reverse the polarization.[93] Contrary to the continuous ferroelectric medium, Lee et al. showed that ferroelectric nanocapacitors, which were physically separated, were individually addressable by a scanning probe microscopy

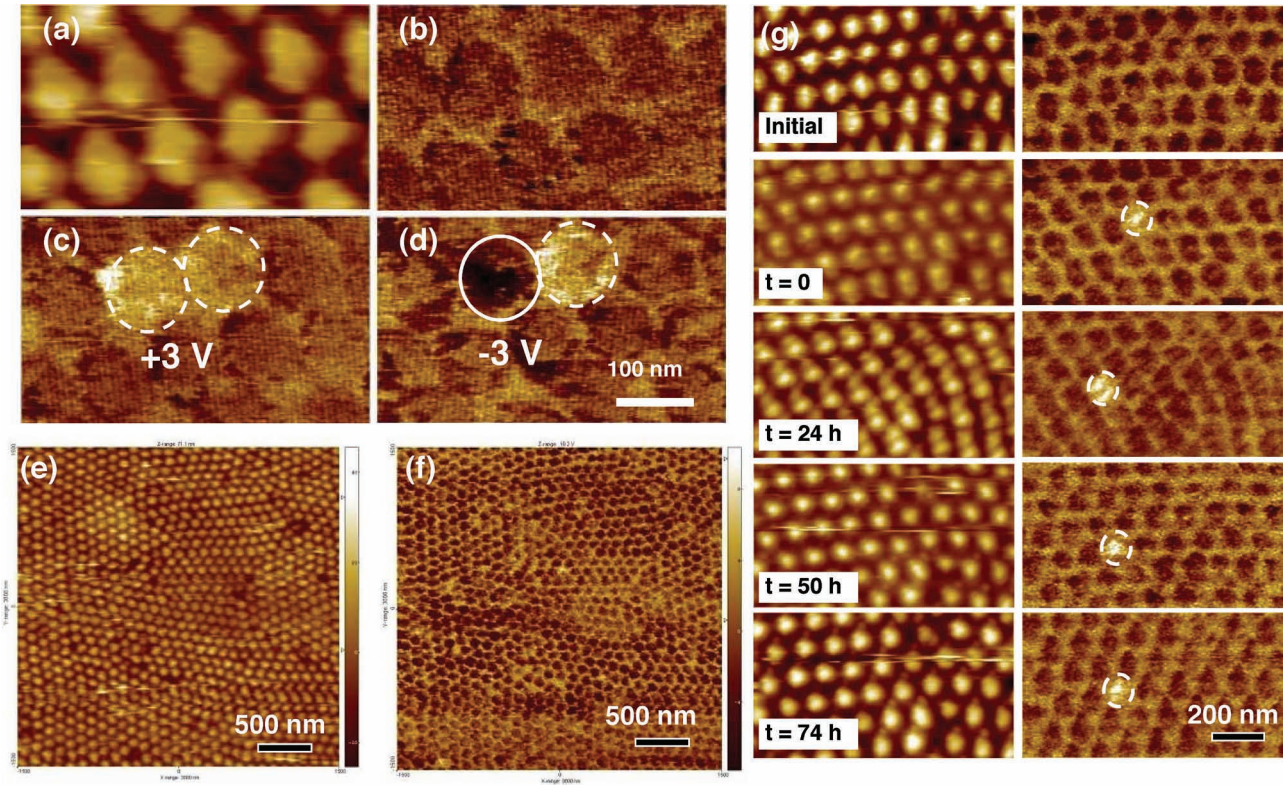

Figure 8. Topography (a) and PFM images (b–d) of PZT nanocapacitors: b) initial state, c) after applying +3 V to two neighboring nanocapacitors, and d) after back-poling by applying –3 V onto the left-side nanocapacitor. e) Topography and f) PFM image of large area arrays of PZT nanocapacitors. The scan size is 3 μm × 3 μm. g) Topography (left column) and PFM image (right column) obtained after applying +5 V onto one nanocapacitor and recorded at different periods of time. Panels (a–d) reproduced with permission.[64] Panels (e,f) reproduced with permission.[83] Copyright 2010, American Institute of Physics.

(SPM) tip and showed good local switching behavior, enabling one to obtain near Tbit in.$^{-2}$ of memory density.[64] **Figure** 8a–d clearly demonstrate the individual addressability of each PZT nanocapacitor by applying an external electric field via the PFM tip (Figure 8a,b show topographic and piezoresponse images of PZT nanocapacitors before switching, respectively, and Figure 8c,d show after switching). Two neighboring nanocapacitors were switched positively by applying +3 V_{dc} as shown in Figure 8c. Then, one of the nanocapacitors was switched back negatively by applying –3 V_{dc} (Figure 8d). The switching of domains under the external electric field did not affect any other neighboring nanocapacitor. PZT nanocapacitors within an extended 2D array were found to have a uniformity on large area (3 μm × 3 μm) as shown in Figure 8e,f in which *z*-ranges of topography image and piezoresponse image are 71 nm and 18.2 V (a.u.), respectively. In addition, the stability of polarization in PZT nanocapacitors was confirmed by a retention test for a short period of time as shown in Figure 8g. Retention can be defined as the ability of the ferroelectric capacitor to retain the stored charge. Topography (left column) and PFM signal (right column) images are shown in Figure 8g. The initial state is shown in the top images. After switching a single PZT nanocapacitor by applying +5 V_{dc}, the 180° reversed state was recorded at different periods of time. The PZT single nanocapacitor, switched with dc bias, preserved the polarization for 74 h. Although the electrical tests above are not representative for all the properties required for practical data storage devices, successful operation of each nanocapacitor under electric field without any deterioration of properties would shed light on the perspectives of applications of ferroelectric nanocapacitors.

3.3. Switching Dynamics in Film-Type Nanocapacitors

In the application of ferroelectrics to data storage devices, the physical switching of the polarization by applying an external electric field is the basic process. Accordingly it is essential to study the fundamental physics of the domain switching process, that is the kinetics of domain nucleation, domain growth, and its relaxation. PFM is a most helpful technique for such studies in the respect of high spatial resolution, non-destructive measurement, easy access to nanoscale investigation, and application to high-density data storage.[94–98] Many researchers have put much effort into investigating the domain switching behavior in micrometer-scale ferroelectric capacitors by PFM.[99–107] Recently, Gruverman et al. suggested a new approach for the study of domain switching dynamics, so called step-by-step switching in which instant domain configurations at different stages of the polarization reversal process are registered with subsequent imaging. This approach allowed the direct study of nanoscale domain switching dynamics through PFM measurement.[106]

The Kolmogorov–Avrami–Ishibashi (KAI) model is a classical theory based on statistical analysis where nucleation occurs in many different sites and considers the switching process as a phase transformation and rate-limiting parameter. It provides an adequate description of the domain switching dynamics of single crystalline, epitaxially grown, and defect-free ferroelectric films.[108–111] In real ferroelectrics, however, several types of extended defects, including dislocations, domain boundaries, grain boundaries, and oxygen vacancies, exist and therefore the switching behavior does not follow the classical KAI model. Li et al. found that in a ferroelectric epitaxial film with low or zero density of 90° domain walls, the switching behavior well obeys the KAI model. However, in a film with a high density of 90° domain walls, the movement of 180° domain walls was limited, thus the switching kinetics changed to a nucleation-limited model, i.e., non-KAI model.[112] Jo et al. also investigated the polarization switching behavior in (111)-oriented PZT polycrystalline films by pulse measurements. They showed that the experimentally observed switching behavior of domains at the late switching stage deviates from the best fit of the KAI model prediction and is rather fitted well with a Lorentzian distribution. They attributed this result to a local field variation in a disordered system due to dipole defects at domain pinning sites.[113] In addition to macroscopic approaches, Gruverman et al. reported that the switching mechanism of polycrystalline PZT capacitors using the step-by-step PFM approach was found to change from the initial nucleation-dominated process to the lateral domain expansion at later stages, which means that the classical KAI model does not provide sufficient description of the slow switching stage.[101]

The switching dynamics in the nanoscale region of the capacitor size can be also differently considered from the classical KAI model because a single defect may have a tremendous influence on the nucleation and growth of domains even in epitaxial films. Most recently, Kim et al. successfully demonstrated that switching dynamics in film-type ferroelectric nanocapacitors did not comply with the KAI model.[114]

Figure 9a shows a PFM image of 2.5 × 2.5 μm^2 epitaxial PZT microcapacitor in which nucleation occurs randomly at many different places and subsequent polarization switching proceeds via lateral domain wall motion inside the capacitor.[115] In this case, the classical KAI model provides an excellent description of the switching dynamics. However, epitaxial PZT nanocapacitors with a lateral dimension of 70 nm show different switching behavior. As shown in Figure 9b, only one nucleus was observed in the nanocapacitor. Figure 9c shows the respective schematic describing cross-sectional domain structures of the PZT nanocapacitor at different pulse widths. The nucleus was generated at the edge of the nanocapacitor, in the same place in every measuring cycle. Subsequent domain growth proceeds as a 1D lateral domain wall movement towards the inside of the nanocapacitor. It is well-known that domain nucleation most probably occurs in the same sites predetermined by defects located at the film-electrode interface, rather than inside the ferroelectric.[116] The edges of capacitors which form an interface of three different phases (metal, ferroelectric, and air)

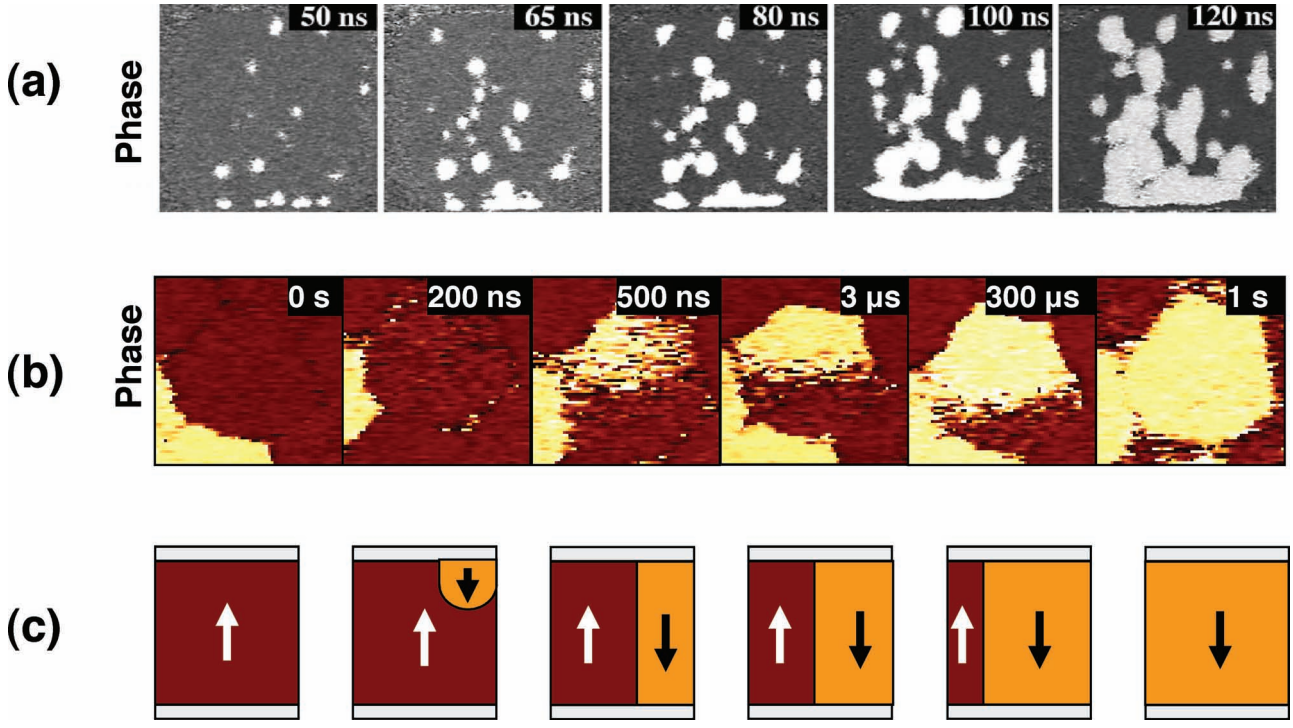

Figure 9. PFM phase images of a) 2.5 μm × 2.5 μm PZT microcapacitor, b) 70 nm film-type PZT nanocapacitors, and c) schematics of domain configurations in (b) under different pulse width and constant applied voltage of +2 V representing cross-sectional PFM images. Panel (a) reproduced with permission.[115] Copyright 2010, American Institute of Physics. Panels (b,c) reproduced with permission.[114] Copyright 2010, American Chemical Society.

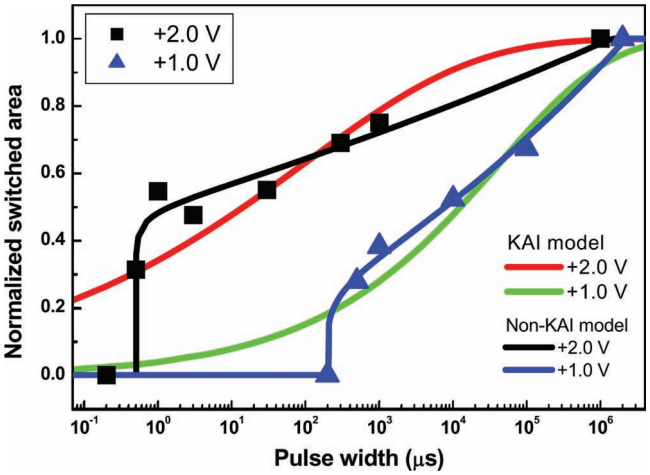

Figure 10. Experimentally obtained data of the pulse width dependence of normalized switched area for +1 V (blue triangles) and +2 V (black squares) and their fitting by classical KAI model (green and red lines) and non-KAI model (blue and black lines). Reproduced with permission.[114] Copyright 2010, American Chemical Society.

are expected to be more prone to defects than the bulk. In addition, the local electric field is higher at the edge of the electrode than inside the capacitor. Therefore, the edge of the capacitor should be the predetermined site for nucleation.

According to the KAI model, the following equation holds;

$$P(t) = 1 - \exp\left[-\left(\frac{t}{t_0}\right)^n\right]$$

where $P(t)$, t_0, and n are the volume fraction of the switched polarization at time t, the characteristic switching time, and a geometric dimension of the domain growth, respectively. The domain growth within PZT nanocapacitors is 1D, thus the value of n should be 1. However, according to the result of the above fitting to the data, i.e., of the time dependence of the switched area obtained experimentally based on the PFM images, shown as blue triangles and black squares for +1 V and +2 V, respectively, n was 0.29 (green line) and 0.19 (red line) for the two different applied voltages of +1 V and +2 V, respectively, as shown in **Figure 10**. An effective dimensionality of the domain growth under 1 is physically impossible, signaling that the classical KAI approach fails to describe the switching process in nanocapacitors.

Regarding the size of the nucleus, it is known that in microcapacitors it is negligible and thus the nucleation process should not significantly influence the switched polarization. However, the size of the nucleus in the nanocapacitor was found to be about 30–50% compared to the entire capacitor area, which indicates that nucleation and growth need to be considered separately. On the other hand, from the relationship of domain wall propagation after nucleation with time, it was also found that the domain wall movement in a nanocapacitor does not have a linear relationship with switching time, but rather a logarithmic one, and the domain wall velocity is not constant.

From these different experimental observations, a new model was derived[114] that describes domain switching dynamics in ferroelectric nanocapacitors via a non-KAI process. Figure 10 shows good approximation of the new model on the switching dynamics of nanocapacitors (blue line and black line for +1 V and +2 V, respectively).

3.4. Cross-Talk Issue in Ferroelectric Nanocapacitors

Unexpected domain wall propagation towards neighboring capacitors under an external electric field, i.e., cross talk, can be a problem in the practical application of film-type nanocapacitors to data storage devices. As previously stated, switching starts at the edge of the nanocapacitor and then the switched domain region propagates towards the inside of the nanocapacitor under the external electric field. When a high electric field is applied to the nanocapacitor higher than a certain critical value, the switching can propagate out of the target nanocapacitor through the continuous ferroelectric medium. The cross-talk effect can be considerable in cases of long pulse width and/or high pulse amplitude. **Figure 11** summarizes the effect of pulse amplitude on the switching stability in film-type nanocapacitors. After back-poling the nanocapacitor (Figure 11a), various pulse voltages with fixed pulse width were applied to the nanocapacitor. Domain switching began to occur at the edge region at +1.5 V of 30 ms (Figure 11b). The switched region was extended by increasing the pulse voltage to +4 V and the domain switching was confined in the nanocapacitor boundary as shown in Figure 11b–e. However, when a higher pulse voltage (+6 V) was applied to the nanocapacitor, the switched region propagated into the outer region, resulting in the domain switching of neighboring nanocapacitors

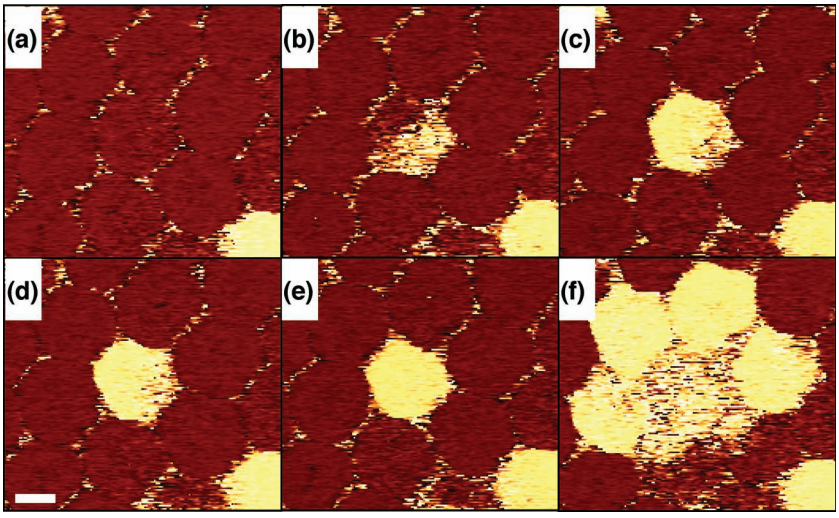

Figure 11. PFM phase images of film-type nanocapacitors with a size of 70 nm. Scale-bar in (d) is 50 nm. After applying –4 V and 40 ms for back poling, various voltages from +1.5 to +6 V were applied to the center capacitor under constant pulse width (30 ms).

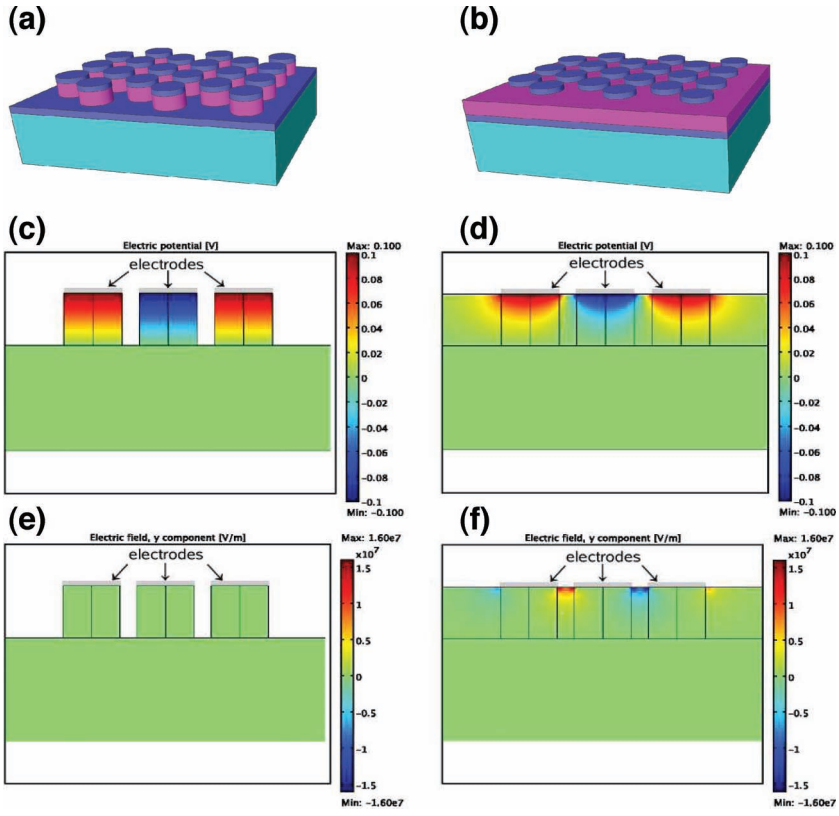

Figure 12. Schematics of a) island-type nanocapacitors and b) film-type nanocapacitors and FEM calculations of respective nanocapacitors. c,d) Electrical potential distribution and e,f) in-plane electric field distribution.

and even a second neighboring nanocapacitor. This domain switching behavior is repeated during the operation under the same switching conditions.

A finite element method (FEM) calculation was carried out in order to investigate the electric field distribution in the two different types of ferroelectric nanocapacitor systems: one is physically separated into island-type nanocapacitors (**Figure 12**a) and the other is a continuous film-type nanocapacitor array (Figure 12b). Voltages of –0.1 V and +0.1 V were applied to the top electrodes of the outer capacitors and of the inner capacitor, respectively. The bottom of both island and film-type nanocapacitors has an electrical potential of 0.0 V. Both nanocapacitors have a relative permittivity of $\varepsilon_r = 150$ (for PZT). The electrical potential and the in-plane component of the electrical field are shown in Figure 12c,e for electrodes on island-type nanocapacitors and in Figure 12d,f for electrodes on film-type nanocapacitors, respectively. From the simulation, it is obvious that a uniform electric field distribution can be generated in physically separated island-type PZT nanocapacitors, leading to an effective focusing of the electric field on the nanocapacitor, a homogeneous domain switching behavior, and good piezoelectric properties. Moreover, in the island-type nanocapacitors the interference of the electric field through that of the neighboring nanocapacitors can be avoided, as observed in the PFM experiment. It can be concluded that island-type ferroelectric nanocapacitors would be of use for practical application to ferroelectric data storage devices.

4. Conclusion

For the realization of ultrahigh-density ferroelectric data storage devices and the clear understanding of the ferroelectric size effect, much effort has been made to develop a robust approach to fabricate structurally well-defined arrays of nanostructured ferroelectrics. For the last decade, considerable advances in the fabrication and characterization of ferroelectric nanostructures have been achieved to an extent that extensive investigations on the structure–property relationships became possible. This Review briefly summarizes the research, including the merits and demerits, of the conventional fabrication methods for ferroelectric nanostructures. The discussion further focuses on newly developed stencil-based growth of ferroelectric nanocapacitors, which allows one not only to obtain 2D-ordered arrays of single crystalline nanostructured ferroelectrics but also to investigate structure–property relationships, i.e., strain-induced domain evolution, its implications on the electric properties, a new phenomenological model for domain dynamics, and cross-talk. These results should be applicable to a wide range of functional oxides in addition to ferroelectrics, e.g., to study domain dynamics in nanoscale multiferroics or potential applications of nanosized oxide capacitors for resistive memory (ReRAM) devices.

Acknowledgements

The authors are thankful to Andriy Lotnyk (Kiel), Markus Andreas Schubert (Frankfurt/Oder), Stephan Senz (Halle), Valanoor Nagarajan (UNSW, Australia), and Sunggi Baik (POSTECH, Korea) for their encouraging discussions and fruitful cooperations and to Volker Schmidt (Halle) for his careful reading of the manuscript. This work was funded by the Max Planck Society, the German Research Foundation DFG (SFB 762), and Future-based Technology Development Program (Nano Fields) through the National Research Foundation of Korea (NRF) funded by the Ministry of Education, Science and Technology (Grant No. 20100029332). Y.K. acknowledges the financial support of the Alexander von Humboldt Foundation.

Received: June 15, 2011
Revised: July 15, 2011
Published online: September 15, 2011

[1] J. Valasek, *Phys. Rev.* **1920**, *15*, 537.
[2] A. R. v. Hippel, *In Dielectrics and Waves*, Wiley, New York **1954**.
[3] O. Auciello, J. F. Scott, R. Ramesh, *Phys. Today* **1998**, *51*, 22.
[4] J. F. Scott, C. A. P. De Araujo, *Science* **1989**, *246*, 1400.
[5] J. F. Scott, *Ferroelectric Memories*, Springer-Verlag, New York **2000**.
[6] R. Waser, *Nanoelectronics and Information Technology: Advanced Electronic Materials and Novel Devices*, Wiley-VCH, Berlin **2005**.

[7] K. Uchino, *Ferroelectric Devices*, Decker, New York **2000**.
[8] M. Dawber, K. M. Rabe, J. F. Scott, *Rev. Mod. Phys.* **2005**, *77*, 1083.
[9] J. F. Scott, *Science* **2007**, *315*, 954.
[10] V. Nagarajan, J. Junquera, J. Q. He, C. L. Jia, R. Waser, K. Lee, Y. K. Kim, S. Baik, T. Zhao, R. Ramesh, P. Ghosez, K. M. Rabe, *J. Appl. Phys.* **2006**, *100*, 051609.
[11] C. Lichtensteiger, J. M. Triscone, J. Junquera, P. Ghosez, *Phys. Rev. Lett.* **2005**, *94*.
[12] J. Junquera, P. Ghosez, *Nature* **2003**, *422*, 506.
[13] V. Nagarajan, I. G. Jenkins, S. P. Alpay, H. Li, S. Aggarwal, L. Salamanca-Riba, A. L. Roytburd, R. Ramesh, *J. Appl. Phys.* **1999**, *86*, 595.
[14] M. Stengel, D. Vanderbilt, N. A. Spaldin, *Nat. Mater.* **2009**, *8*, 392.
[15] C. L. Jia, S. B. Mi, K. Urban, I. Vrejoiu, M. Alexe, D. Hesse, *Nat. Mater.* **2008**, *7*, 57.
[16] S. K. Streiffer, J. A. Eastman, D. D. Fong, C. Thompson, A. Munkholm, M. V. R. Murty, O. Auciello, G. R. Bai, G. B. Stephenson, *Phys. Rev. Lett.* **2002**, *89*, 067602.
[17] D. D. Fong, G. B. Stephenson, S. K. Streiffer, J. A. Eastman, O. Auciello, P. H. Fuoss, C. Thompson, *Science* **2004**, *304*, 1650.
[18] R. Waser, A. Rüdiger, *Nat. Mater.* **2004**, *3*, 81.
[19] Y. G. Wang, W. L. Zhong, P. L. Zhang, *Phys. Rev. B* **1995**, *51*, 5311.
[20] Y. G. Wang, W. L. Zhong, P. L. Zhang, *Phys. Rev. B* **1995**, *51*, 17235.
[21] R. Kretschmer, K. Binder, *Phys. Rev. B* **1979**, *20*, 1065.
[22] S. P. Li, J. A. Eastman, Z. Li, C. M. Foster, R. E. Newnham, L. E. Cross, *Phys. Lett. A* **1996**, *212*, 341.
[23] I. Vrejoiu, M. Alexe, D. Hesse, U. Gösele, *J. Vac. Sci. Technol. B* **2009**, *27*, 498.
[24] M. Alexe, C. Harnagea, D. Hesse, *J. Electroceram.* **2004**, *12*, 69.
[25] A. Rudiger, T. Schneller, A. Roelofs, S. Tiedke, T. Schmitz, R. Waser, *Appl. Phys. A: Mater. Sci. Process.* **2005**, *80*, 1247.
[26] C. S. Ganpule, A. Stanishevsky, Q. Su, S. Aggarwal, J. Melngailis, E. Williams, R. Ramesh, *Appl. Phys. Lett.* **1999**, *75*, 409.
[27] V. Nagarajan, A. Stanishevsky, R. Ramesh, *Nanotechnology* **2006**, *17*, 338.
[28] V. Nagarajan, A. Roytburd, A. Stanishevsky, S. Prasertchoung, T. Zhao, L. Chen, J. Melngailis, O. Auciello, R. Ramesh, *Nat. Mater.* **2003**, *2*, 43.
[29] A. Schilling, D. Byrne, G. Catalan, K. G. Webber, Y. A. Genenko, G. S. Wu, J. F. Scott, J. M. Gregg, *Nano Lett.* **2009**, *9*, 3359.
[30] M. Alexe, C. Harnagea, D. Hesse, U. Gösele, *Appl. Phys. Lett.* **1999**, *75*, 1793.
[31] M. Alexe, C. Harnagea, D. Hesse, U. Gösele, *Appl. Phys. Lett.* **2001**, *79*, 242.
[32] M. Alexe, C. Harnagea, W. Erfurth, D. Hesse, U. Gösele, *Appl. Phys. A: Mater. Sci. Process.* **2000**, *70*, 247.
[33] S. Bühlmann, B. Dwir, J. Baborowski, P. Muralt, *Appl. Phys. Lett.* **2002**, *80*, 3195.
[34] K. Lee, S. Baik, *Ann. Rev. Mater. Res.* **2006**, *36*, 81.
[35] C. Harnagea, M. Alexe, J. Schilling, J. Choi, R. B. Wehrspohn, D. Hesse, U. Gösele, *Appl. Phys. Lett.* **2003**, *83*, 1827.
[36] A. Seifert, A. Vojta, J. S. Speck, F. F. Lange, *J. Mater. Res.* **1996**, *11*, 1470.
[37] M. Alexe, D. Hesse, *J. Mater. Sci.* **2006**, *41*, 1.
[38] I. Szafraniak, M. W. Chu, C. Harnagea, R. Scholz, D. Hesse, M. Alexe, *Integr. Ferroelectr.* **2004**, *61*, 231.
[39] I. Szafraniak, S. Bhattacharyya, C. Harnagea, R. Scholz, M. Alexe, *Integr. Ferroelectr.* **2004**, *68*, 279.
[40] A. Roelofs, T. Schneller, K. Szot, R. Waser, *Nanotechnology* **2003**, *14*, 250.
[41] I. Szafraniak, C. Harnagea, R. Scholz, S. Bhattacharyya, D. Hesse, M. Alexe, *Appl. Phys. Lett.* **2003**, *83*, 2211.
[42] A. Roelofs, I. Schneller, K. Szot, R. Waser, *Appl. Phys. Lett.* **2002**, *81*, 5231.
[43] H. Fujisawa, M. Okaniwa, H. Nonomura, M. Shimizu, H. Niu, *J. Eur. Ceram. Soc.* **2004**, *24*, 1641.
[44] M. Shimizu, N. Nonomura, H. Fujisawa, H. Niu, K. Honda, *Integr. Ferroelectr.* **2004**, *62*, 109.
[45] H. Han, K. Lee, W. Lee, M. Alexe, D. Hesse, S. Baik, *J. Mater. Sci.* **2009**, *44*, 5167.
[46] M. W. Chu, I. Szafraniak, R. Scholz, C. Harnagea, D. Hesse, M. Alexe, U. Gosele, *Nat. Mater.* **2004**, *3*, 87.
[47] S. H. Ahn, S. K. Choi, *Appl. Phys. Lett.* **2008**, *93*, 113102.
[48] I. Szafraniak, M. Alexe, *Ferroelectrics* **2003**, *291*, 19.
[49] S. Bühlmann, P. Muralt, S. Von Allmen, *Appl. Phys. Lett.* **2004**, *84*, 2614.
[50] W. Lee, M. Alexe, K. Nielsch, U. Gösele, *Chem. Mater.* **2005**, *17*, 3325.
[51] S. K. Lee, W. Lee, M. Alexe, K. Nielsch, D. Hesse, U. Gösele, *Appl. Phys. Lett.* **2005**, *86*, 152906.
[52] S. K. Lee, D. Hesse, M. Alexe, W. Lee, K. Nielsch, U. Gösele, *J. Appl. Phys.* **2005**, *98*, 124302.
[53] W. H. Ma, D. Hesse, U. Gösele, *Small* **2005**, *1*, 837.
[54] W. H. Ma, D. Hesse, *Appl. Phys. Lett.* **2004**, *85*, 3214.
[55] H. Han, R. Ji, Y. J. Park, S. K. Lee, G. Le Rhun, M. Alexe, K. Nielsch, D. Hesse, U. Gösele, S. Baik, *Nanotechnology* **2009**, *20*, 015301.
[56] S. Clemens, T. Schneller, A. van der Hart, F. Peter, R. Waser, *Adv. Mater.* **2005**, *17*, 1357.
[57] S. Kronholz, S. Rathgeber, S. Karthäuser, H. Kohlstedt, S. Clemens, T. Schneller, *Adv. Funct. Mater.* **2006**, *16*, 2346.
[58] Y. Kim, H. Han, Y. Kim, W. Lee, M. Alexe, S. Baik, J. K. Kim, *Nano Lett.* **2010**, *10*, 2141.
[59] H. Nonomura, H. Fujisawa, M. Shimizu, H. Niu, K. Honda, *Jpn. J. Appl. Phys.* **2003**, *42*, 5918.
[60] M. W. Chu, I. Szafraniak, D. Hesse, M. Alexe, U. Gösele, *Phys. Rev. B* **2005**, *72*.
[61] P. R. Evans, X. H. Zhu, P. Baxter, M. McMillen, J. McPhillips, F. D. Morrison, J. F. Scott, R. J. Pollard, R. M. Bowman, J. M. Gregg, *Nano Lett.* **2007**, *7*, 1134.
[62] E. J. Mele, *Am. J. Phys.* **2001**, *69*, 557.
[63] S. V. Kalinin, E. Karapetian, M. Kachanov, *Phys. Rev. B* **2004**, *70*.
[64] W. Lee, H. Han, A. Lotnyk, M. A. Schubert, S. Senz, M. Alexe, D. Hesse, S. Baik, U. Gösele, *Nat. Nanotechnol.* **2008**, *3*, 402.
[65] A. P. Li, F. Muller, A. Birner, K. Nielsch, U. Gösele, *J. Appl. Phys.* **1998**, *84*, 6023.
[66] D. Damjanovic, *Rep. Prog. Phys.* **1998**, *61*, 1267.
[67] M. E. Lines, A. M. Glass, *Principles and Applications of Ferroelectrics and Related Materials*, Clarendon Press, Oxford **1982**.
[68] W. Pompe, X. Gong, Z. Suo, J. S. Speck, *J. Appl. Phys.* **1993**, *74*, 6012.
[69] S. Nambu, D. A. Sagala, *Phys. Rev. B* **1994**, *50*, 5838.
[70] R. Ramesh, T. Sands, V. G. Keramidas, *Appl. Phys. Lett.* **1993**, *63*, 731.
[71] Y. Xu, *Ferroelectric Materials and Their Applications*, Elsevier Science, Amsterdam **1993**.
[72] K. S. Lee, J. H. Choi, J. Y. Lee, S. Baik, *J. Appl. Phys.* **2001**, *90*, 4095.
[73] S. V. Kalinin, S. Jesse, B. J. Rodriguez, K. Seal, A. P. Baddorf, T. Zhao, Y. H. Chu, R. Ramesh, E. A. Eliseev, A. N. Morozovska, B. Mirman, E. Karapetian, *Jpn. J. Appl. Phys.* **2007**, *46*, 5674.
[74] S. V. Kalinin, A. N. Morozovska, L. Q. Chen, B. J. Rodriguez, *Rep. Prog. Phys.* **2010**, *73*, 056502.
[75] S. Jesse, B. J. Rodriguez, S. Choundhury, A. P. Baddorf, I. Vrejoiu, D. Hesse, M. Alexe, E. A. Eliseev, A. N. Morozovska, J. Zhang, L. Q. Chen, S. V. Kalinin, *Nat. Mater.* **2008**, *7*, 209.
[76] B. J. Rodriguez, S. Jesse, M. Alexe, S. V. Kalinin, *Adv. Mater.* **2008**, *20*, 109.
[77] A. Gruverman, *J. Mater. Sci.* **2009**, *44*, 5182.

[78] A. Gruverman, A. Kholkin, *Rep. Prog. Phys.* **2006**, *69*, 2443.
[79] A. Gruverman, D. Wu, H. J. Fan, I. Vrejoiu, M. Alexe, R. J. Harrison, J. F. Scott, *J. Phys.: Condens. Matter* **2008**, *20*, 342201.
[80] A. Schilling, R. M. Bowman, G. Catalan, J. F. Scott, J. M. Gregg, *Nano Lett.* **2007**, *7*, 3787.
[81] A. Schilling, D. Byrne, G. Catalan, K. G. Webber, Y. A. Genenko, G. S. Wu, J. F. Scott, J. M. Gregg, *Nano Lett.* **2009**, *9*, 3359.
[82] G. Catalan, A. Schilling, J. F. Scott, J. M. Gregg, *J. Phys.: Condens. Matter* **2007**, *19*, 132201.
[83] H. Han, Y. J. Park, S. Baik, W. Lee, M. Alexe, D. Hesse, U. Gösele, *J. Appl. Phys.* **2010**, *108*, 044102.
[84] K. Lee, H. Yi, W. H. Park, Y. K. Kim, S. Baik, *J. Appl. Phys.* **2006**, *100*, 051615.
[85] F. Xu, S. Trolier-McKinstry, W. Ren, B. M. Xu, Z. L. Xie, K. J. Hemker, *J. Appl. Phys.* **2001**, *89*, 1336.
[86] A. L. Kholkin, E. K. Akdogan, A. Safari, P. F. Chauvy, N. Setter, *J. Appl. Phys.* **2001**, *89*, 8066.
[87] K. S. Lee, Y. K. Kim, S. Baik, J. Kim, I. S. Jung, *Appl. Phys. Lett.* **2001**, *79*, 2444.
[88] Y. K. Kim, H. Morioka, R. Ueno, S. Yokoyama, H. Funakubo, *Appl. Phys. Lett.* **2005**, *86*, 212905.
[89] Y. K. Kim, H. Morioka, R. Ueno, S. Yokoyama, H. Funakubo, K. Lee, S. Baik, *Appl. Phys. Lett.* **2006**, *88*, 252904.
[90] G. Le Rhun, I. Vrejoiu, L. Pintilie, D. Hesse, M. Alexe, U. Gösele, *Nanotechnology* **2006**, *17*, 3154.
[91] V. Nagarajan, *Appl. Phys. Lett.* **2005**, *87*, 242905.
[92] J. Woo, S. Hong, N. Setter, H. Shin, J. U. Jeon, Y. E. Pak, K. No, *J. Vac. Sci. Technol. B* **2001**, *19*, 818.
[93] N. Ng, R. Ahluwalia, H. B. Su, F. Boey, *Acta Mater.* **2009**, *57*, 2047.
[94] K. Terabe, M. Nakamura, S. Takekawa, K. Kitamura, S. Higuchi, Y. Gotoh, Y. Cho, *Appl. Phys. Lett.* **2003**, *82*, 433.
[95] A. Gruverman, in *Encycolpedia of Nanoscience and Nanotechnology*, Vol. *3* (Ed: H. S. Nalwa), American Scientific Publisher, Los Angeles **2004**, 359.
[96] S. Hong, J. Woo, H. Shin, J. U. Jeon, Y. E. Pak, E. L. Colla, N. Setter, E. Kim, K. No, *J. Appl. Phys.* **2001**, *89*, 1377.
[97] S. Hong, N. Park, *Scanning Probe Microscopy: Electrical and Electromechanical Phenomena at the Nanoscale*, Springer, Berlin **2006**.
[98] S. V. Kalinin, D. A. Bonnell, *Phys. Rev. B* **2002**, *65*, 125408.
[99] S. Hong, E. L. Colla, E. Kim, D. V. Taylor, A. K. Tagantsev, P. Muralt, K. No, N. Setter, *J. Appl. Phys.* **1999**, *86*, 607.
[100] P. Paruch, T. Tybell, J. M. Triscone, *Appl. Phys. Lett.* **2001**, *79*, 530.
[101] A. Gruverman, O. Auciello, H. Tokumoto, *Ann. Rev. Mater. Sci.* **1998**, *28*, 101.
[102] J. Li, B. Nagaraj, H. Liang, W. Cao, C. H. Lee, R. Ramesh, *Appl. Phys. Lett.* **2004**, *84*, 1174.
[103] B. J. Rodriguez, R. J. Nemanich, A. Kingon, A. Gruverman, S. V. Kalinin, K. Terabe, X. Y. Liu, K. Kitamura, *Appl. Phys. Lett.* **2005**, *86*, 012609.
[104] A. L. Kholkin, C. Wutchrich, D. V. Taylor, N. Setter, *Rev. Sci. Instrum.* **1996**, *67*, 1935.
[105] C. Dehoff, B. J. Rodriguez, A. I. Kingon, R. J. Nemanich, A. Gruverman, J. S. Cross, *Rev. Sci. Instrum.* **2005**, *76*, 023708.
[106] A. Gruverman, B. J. Rodriguez, C. Dehoff, J. D. Waldrep, A. I. Kingon, R. J. Nemanich, J. S. Cross, *Appl. Phys. Lett.* **2005**, *87*, 082902.
[107] A. Gruverman, D. Wu, J. F. Scott, *Phys. Rev. Lett.* **2008**, *100*, 097601.
[108] Y. Ishibashi, Y. Takagi, *J. Phys. Soc. Jpn.* **1971**, *31*, 506.
[109] M. Avrami, *J. Chem. Phys.* **1939**, *7*, 1103.
[110] A. N. Kolmogorov, *Izv. Akad. Nauk USSR; Ser. Math* **1937**, *3*, 355.
[111] Y. Kim, H. Han, B. J. Rodriguez, I. Vrejoiu, W. Lee, S. Baik, D. Hesse, M. Alexe, *J. Appl. Phys.* **2010**, *108*, 042005.
[112] W. Li, M. Alexe, *Appl. Phys. Lett.* **2007**, *91*, 262903.
[113] J. Y. Jo, H. S. Han, J. G. Yoon, T. K. Song, S. H. Kim, T. W. Noh, *Phys. Rev. Lett.* **2007**, *99*, 267602.
[114] Y. Kim, H. Han, W. Lee, S. Baik, D. Hesse, M. Alexe, *Nano Lett.* **2010**, *10*, 1266.
[115] D. Wu, I. Vrejoiu, M. Alexe, A. Gruverman, *Appl. Phys. Lett.* **2010**, *96*, 112903.
[116] D. J. Kim, J. Y. Jo, T. H. Kim, S. M. Yang, B. Chen, Y. S. Kim, T. W. Noh, *Appl. Phys. Lett.* **2007**, *91*, 132903.